INSTITUTE OF PHYSICS PUBLISHING JOURNAL OF PHYSICS: CONDENSED MATTER

J. Phys.: Condens. Matter **14** (2002) 6081–6107 PII: S0953-8984(02)35563-2

Computer simulation by the quantum mechanical time-dependent wavepacket method, especially for atom/molecule–solid-surface interaction

G Varga[1]

Budapest University of Technology and Economics, Department of Physics, Budafoki út. 8, Budapest, H-1111, Hungary

E-mail: vargag@phy.bme.hu

Received 5 April 2002
Published 31 May 2002
Online at stacks.iop.org/JPhysCM/14/6081

Abstract

Thermal energy atomic scattering (TEAS) on solid surfaces forms the basis of a useful experimental method for obtaining information about the structure, disorder and phonon spectra of the solid surface. The probe particles (usually He atoms) can spend a relatively long time near the solid surface in the interaction region. The dynamics of the interaction processes cannot be investigated directly at present. However, an appropriate physical model of the interaction fitted to the intensity distribution of the scattering may be suitable for use in investigating the interaction processes theoretically, by computer simulation. The present work emphasizes this computer simulation method. For an actual computer simulation, the detector region TEAS experimental method must be appropriate. Moreover a theoretical model for the TEAS (e.g. a one-particle quantum mechanical wavepacket model governed by the time-dependent Schrödinger equation (TDSE)) and a numerical method for solving the TDSE are necessary.

The state functions of the consecutive time steps provide enough information to produce an 'animation' displaying the dynamics of the interaction processes. An 'animation' is a series of snapshots of e.g. the probability density function (PDF), taken in rapid succession. The sequence of these snapshots provides a 'movie' of the PDF time evolution.

Applications, physical models, numerical solution procedures and simulation techniques relating to the time-dependent wavepacket (TDWP) method are overviewed in the present contribution—especially for the case of TEAS and molecular beam scattering. Several relevant applications of the TDWP method—in the case of TEAS—are discussed (to scattering on ordered, stepped and adsorbed surfaces, the intensity distribution as a function of transfer width, resonant adsorption and trapping, classical and quantum chaos, scattering from vibrating surfaces). Preliminary results on the quantum chaos

[1] http://goliat.eik.bme.hu/∼vargag/

in TEAS are presented for the first time. The theoretical and computational background (the TDWP and coupled channel methods) as well as applications (to diffraction probability, sticking probability, dissociative adsorption, the steering effect, inelastic channels) of six-dimensional molecule/surface dynamics calculations are described.

(Some figures in this article are in colour only in the electronic version)

1. Introduction

Thermal energy atomic scattering (TEAS) on solid surfaces provides the basis of an efficient method for exploring the surface topology, phonon spectra, surface disorder and the probe particle–solid-surface interaction. Molecular beam scattering (MBS) can be used to explore molecule–solid-surface reactions. TEAS and MBS investigations usually require a quantum mechanical model to describe the physical phenomena. Classical and semiclassical models are also used in the literature to characterize TEAS and MBS. Since the interaction of the atom (e.g. He) with the solid-surface system changes abruptly near the classical turning point, the classical trajectories are washed out. This supports the case for application of an appropriate quantum mechanical model. Probe particles of larger mass and higher energy lead to weaker quantum effects and semiclassical and classical models then come to the fore.

The traditional quantum mechanical models of TEAS suppose periodic solid surfaces. A successful and simple quantum mechanical model, the so-called hard-corrugated-wall (HCW) model, was developed by García [1]. The probe particle interaction potential is zero above the surface but infinite at the corrugated surface. The state function at the solid surface is equal to zero due to the infinite-potential wall. On this assumption, solution of a complex linear system of equations will lead to the diffraction pattern in the detector region.

García's method has been improved by Varga and Füstöss and by Stoll *et al* [2–4]. The convergence and the stability have also been improved. The symmetry of the solid surface has been considered [5] too; this led to the development of an efficient inverse scattering algorithm [6, 7]. An integral equation solution method was introduced by Salanon and Armand [8].

The soft-corrugated-wall model was the next quantum mechanical model to be developed. In executing the numerical solution method, the time-independent Schrödinger equation (TISE) was applied to a series of reciprocal lattices of the solid surfaces. This method provided a system of closely coupled differential equations. Its solution gives the scattering amplitude (CCGM method [9]). In the case of smooth surfaces (e.g. certain metal surfaces) a perturbation theory—the so-called distorted Born approximation—also provides an efficient method [10]. The details of and further references to TEAS theory and experiments can be found in [11, 12].

A real surface contains different disorder types, e.g. adatoms, vacancies, steps. The surface disorders disrupt the perfect periodicity. This hinders the application of the above-mentioned traditional methods. The wavepacket method is appropriate for eliminating this problem. In the framework of the time-dependent wavepacket (TDWP) method, the atomic/molecular beam is described as an ensemble of independent particles represented by an appropriate Gaussian wavepacket. The wavepacket velocity and spread ensure the right average beam energy and the monochromaticity, respectively. The surface can be disordered because the wavepacket time propagation is governed by a time-dependent Schrödinger equation (TDSE) and surface periodicity is not exploited in the numerical solution. The physical quantities can be computed

from the state function (see the details in the appendix). It is a relevant property of the TDWP method that the time evolution of the physical phenomena is reflected by the wavepacket propagation. As a result of this, during the process the state of the atomic beam is known beyond the detector region, too. By means of the TDWP method one can also calculate the dynamics of the interaction region near the classical turning point, where the measurement of the atomic beam state is impossible at present.

Section 2 reviews some research areas of the TDWP method. The numerical tools required in the TDWP method are discussed in section 3. In section 4 computer animation as a computer simulation method (CSM) is introduced. The TDWP method is described in sections 5 and 6 for the cases of TEAS and MBS, respectively, together with several applications. The conclusions are given in section 7.

2. Recent applications and development of the TDWP method

It is important to mention that the details of the different applications are not treated thoroughly in this section; the reader is referred to the references.

Recently, the TDWP method was used to describe *reactive scattering*, to calculate the microcanonical cumulative reaction probability and probabilities of molecular transitions in time-dependent fields and to decouple the reactant and product parts of the wavefunction in state-to-state reactive scattering calculations. An accurate TDWP calculation for the O(D) + DCl reaction was carried out employing a potential energy surface (PES) [13]. Apparent differences are found in the energy dependence of the reaction probability and the magnitudes of the rate constants between the O(D) + DCl reaction and the isotopic O(D) + HCl reaction [14]. These differences are attributed mainly to kinematic effects. Classical and quantum dynamics computations of the collinear PES for the reaction of Li with H_2 were executed by Clarke *et al* [15]. The specific features of the potential were analysed for some indicative configurations and classical trajectory calculations were carried out for a special collinear arrangement. In the case of collinear arrangement, quantum TDWP calculations were also performed and the two sets of results are found to be in rather good accord with each other. Zhang *et al* [16] carried out a time-dependent quantum wavepacket calculation for the HD+CN reaction. That was done using a new PES with the potential-averaged five-dimensional model. Discrete variable representations for the radial coordinate and a renormalized angular quadrature scheme were applied in the wavepacket propagation in order to save computer memory. Domenico *et al* [17] presented a TDWP approach for computing the probabilities of reaction and collision-induced dissociation for $H_2 + H_2$. It was found that the method provides more accurate results than a time-independent hyperspherical treatment. The time-dependent quantum wavepacket method was applied by Zhang *et al* [18] to study the dynamics of the ion–molecule reaction of $N^+ + H_2$ on a special PES.

Atomic phenomena in *bichromatic laser fields* can be described by the wavepacket method, as the atomic electron is modelled by a wavepacket [19]. The computation demands the solution of the one- and three-dimensional TDSEs.

Ferrero and Robicheaux [20] presented a theory for the scattering of a *short electron pulse* from a molecular wavepacket. They investigated the transition between two electronic states and showed how transition probabilities as a function of internal nuclear positions can be obtained. A pulsed electron beam can also be used to control the probabilities of transition to different electronic levels, obtained by direct numerical solution of the TDSE.

Nuclear wavepackets are prepared using a chirped femtosecond laser pulse depending on the chirp parameter; they exhibit different vibrational dynamics [21]. Using the potassium dimer, it can be shown that time-resolved photoelectron spectroscopy is able to map the

characteristics of the nuclear probability density and to distinguish densities obtained from excitations using differently chirped pulses. Numerical calculations provide information about the uncertainties of wavepackets, which can be directly obtained from the spectra.

Three-dimensional wavepacket calculations on the O_3 molecule have been performed for the case where the total angular momentum equals zero [22]. The split operator (SPO) propagator and the fast Fourier transform method in hyperspherical coordinates are used in order to follow the quantum dynamics of *photodissociation*. The effect of the finite lifetime of the excited state has been studied, in an effort to explain the disagreement between the theoretical calculations and experimental data.

Time-dependent photodissociation resonances were investigated in the case of a collinear CO_2 system using the wavepacket method [23]. The excited- and ground-state wavepacket behaviour caused by frequency chirping of a femtosecond laser pulse in H_2 photodissociation has been investigated using a time-dependent method [24]. Control over wavepacket processes is the foundation of laser control of chemical reaction dynamics. The critical stage in a chemical reaction occurs within 10^{-12} s. When femtosecond laser technology emerged, it became possible to manipulate and control molecular processes in this key stage. The most important task is to solve the coupled TDSEs.

The *photoabsorption* spectra of the molecules HI and DI were computed using *ab initio* potential curves and transition dipole moments [25]. Partial absorption cross-sections and an excited spin–orbit state of iodine were calculated using the TDWP formalism, as a function of the excitation energy. Good agreement with experimental data was obtained. The wavefunctions and potentials were represented on a set of equally spaced grid points and the Schrödinger equation was solved using the SPO method.

Mahapatra *et al* [26] investigated the *non-adiabatic wavepacket dynamics* for coupled electronic states of NO_2 on the basis of new *ab initio* PESs. The elements of the vibronic Hamiltonian are weakly varying functions of the nuclear coordinates and the kinetic energy operator can be taken as diagonal.

Sweeney and De Vries [27] applied the SPO method of solution to the TDSE for two-dimensional *Rutherford scattering* and the wavefunction was visualized as a function of time.

De Raedt [28–30] focused on simulating the quantum mechanical motion of *electrons in nanoscale devices*. Supplemented by computer animation techniques, the simulation provides clear insight into the physical behaviour. The Aharonov–Bohm effect has been simulated by a wavepacket method, too.

Andersson and Stenholm [31] investigated cooling and trapping techniques for atoms, allowing the fabrication of genuinely microscopic *quantum wires and dots for individual particles*. The physical features of a structure were discussed and illustrated with wavepacket simulations.

Márk *et al* [32–35] executed a thorough computer simulation of *scanning tunnelling microscopy* (STM) experiments on carbon nanotubes. The three-dimensional wavepacket method was applied to explore the dynamics of the electron tunnelling between a realistic STM tip and carbon nanotubes. The time propagation of the probability density function (PDF) in the nanotube was rendered as a computer animation and the electron dwell time distribution. The simulation results were compared to experimental ones, too.

Further fruitful applications of the TDWP method were investigations of *atom/molecule–solid-surface interactions* by means of TEAS and MBS. Details can be seen in sections 5 and 6, respectively.

3. Numerical solution methods in the TDWP method

If the quantum system is small and if it has dissociative or tunnelling coordinates, the grid method is very convenient to use, as a direct procedure which avoids state expansion. Nowadays six-dimensional computations can be executed in several cases. Of course, the degree of freedom depends on the physical situation that can be handled without a supercomputer. For atom/molecule–solid-surface scattering and interaction, grid methods can be extremely useful. The methods are accurate and suitable for the investigation of complex systems, as is shown in section 2. The numerical procedure for the solution of the Schrödinger equation can be divided into the following steps:

(a) *An appropriate initial wavefunction has to be chosen*. The average energy and energy spread of the atomic beam must be considered. It is a good idea to choose a Gaussian wavepacket for determining the intensity distribution of the TEAS. However, the composition of the initial wavepacket is a crucial question that depends on the physical phenomena which we want to investigate. For example, if the dynamics of diatomic molecule scattering has to be analysed, the initial wavefunction should be a sum of the incoming plane waves in the detector region where the particle moves freely. The plane waves should be products of the following: a plane wave perpendicular to the surface, a function describing parallel translational motion, a vibrational wavefunction for a molecule in the appropriate rovibrational state and a spherical harmonic function of the appropriate rotational state. This ansatz provides the possibility of describing rovibrational and rotational probabilities of different states, which are identified by certain quantum numbers. That is, the right initial wavefunction should span the physical space of the processes. This type of initial wavefunction construction speeds up the convergence of the numerical procedure, and decreases the computational effort required.

(b) *The boundary condition has to be chosen*. A large enough subspace has to be chosen in order that the wavefunction should be zero at boundary points throughout the whole physical process. If this is not realizable—e.g. because of the computer memory requirements—absorbing [60, 62] or cutting techniques [93, 148] must be applied to the wavefunction.

(c) *A method has to be applied to construct the Hamilton operator*. It can be calculated by a finite-difference method, a finite-element method or a pseudo-spectral method. The fast Fourier transformation (FFT) is an efficient pseudo-spectral algorithm [36–39]. FFT demands periodic boundary conditions, but the convergence speed is exponential in the number of terms. Unfortunately, the convergence of the finite-difference method is only polynomial. The finite-element method has good convergence characteristics and the boundary conditions can be built easily; however, the computer code generation of the mesh is complicated [40, 41].

(d) *One has to choose a time-propagation approach*. The global operator scheme—e.g. a Chebyshev scheme—determines the time propagator for a longer time interval [42, 43]. These methods can be extremely accurate; however, they are not recommended foe time-dependent interaction energy problems and for wavefunctions which occupy very small spectral ranges in relation to the spectral range of the grid. The Chebyshev scheme does not preserve the norm, does not conserve energy and is unstable as regards grid density. The finite-difference scheme for the time propagator—the second-order-difference (SOD) scheme is the simplest—is based on the Taylor series [44]. The SOD scheme preserves the norm, conserves energy, but is unstable as regards the grid density and time step. The SPO method divides the Hamiltonian into two different parts [38, 45–49]. The first part is the kinetic energy and the second part is the interaction energy. The approximative formula

contains pure kinetic energy and interaction energy terms. These non-mixed terms can be calculated efficiently by means of an algebraic operation in the momentum space (kinetic energy) and in the real space (interaction energy). Between the momentum space and the real space a 'vice versa' transformation is required (e.g. FFT). Short iterative Lánczos (SIL) propagation is based on generating a set of orthogonal polynomials lying within the subspace, which represents a finite-polynomial approximation to the operator [50–52]. SIL propagation preserves the norm, conserves energy and is stable as regards grid density.

(e) *Error indication is an important task*. The computational accuracy can be controlled by the time symmetry of the TDSE for all of the methods. When one goes back to the time zero, one should get back the starting wavefunction. The difference between the original, initial wavefunction and the computed one can be measured by any norm—e.g. the Euclidean norm—especially focused on the phase error. Other indicators, based on the above descriptions of the different time-propagation methods, can also be found. The Chebyshev method can be controlled using the norm of the wavefunction and the particle average energy. Since the SOD method retains the unity of the wavefunction and conserves energy, these physical quantities are not suitable for indicate the computation accuracy. However, the SOD method is unstable as regards grid density. If the grid density is not large enough, the method is divergent. Because the SPO method does not conserve energy, the average energy as a function of time is a good indicator.

(f) *The wavefunction has to be analysed* to obtain the time propagation of the physical quantities (see the appendix).

Further details of the numerical solution can be found in the following references: Gerber *et al* [53], Kosloff [54], Billing [55], Leforester *et al* [56] and Thaller [57].

3.1. Further development for numerical solution of the TDWP method

Let us give some results that were obtained by new and efficient numerical procedures. The predissociation dynamics of the vibrational eigenstates of hydrogen bromide ions in the first excited electronic states—that occurs via coupling to three repulsive states—has been investigated by direct solution of *four coupled 1D TDSEs* [58]. The analysis shows multi-exponential decay for most of the predissociating vibrational states. The lifetime of these states decreases by several orders of magnitude. The SPO method [38] as well as the integral equation method [59] have been used for determining the propagation of the wavefunctions. An absorbing boundary [60] is used to prevent artificial reflection of the wavefunctions at the edge of the grid.

Dattoli *et al* [61] exploited the formal properties of the evolution operators of the Fokker–Planck and Schrödinger equations. The evolution operators were approximated with special forms *of Laguerre polynomials and Laguerre-based functions*. An advantage offered by the SPO method is that there is no explicit requirement for evaluating the Fourier transform of the initial function. The main disadvantage is that an iteration procedure is unavoidable.

Palao and Muga [62] developed a simple construction of *absorbing potentials* for the case of the TDSE. Complex absorbing potentials are important auxiliary tools in the TDWP method. The traditional role of the absorbing potentials is to lessen the computational burden by avoiding spurious reflections at the edges of the finite 'box' in which the wavepacket is enclosed. If periodic boundary conditions are imposed, they also prevent 'transmission' to the other side of the box. The procedure of using absorbing potentials is based on adding a series of equal-length complex square barriers and optimizing their real and imaginary parts to achieve maximum absorption at a selected set of momenta. The absorption widths obtained are better than other known functional forms for the important low-momentum region. Palao and Muga

have proposed a method for constructing optimized absorbing potentials by combining complex square barriers.

Jiang and Zhao [63] proposed two new propagation schemes for the *quantum time-dependent self-consistent field equations* from a different point of view. If the state of the system under discussion is represented by a multiple-element vector wavefunction, a time-independent quasi-Hamilton operator for the total system can be defined.

Nest *et al* [64] applied the *mapped Fourier method* for scattering problems. The new scheme uses a set of non-equidistant grid points. The key idea is to construct an adaptive grid, with a high grid-point density in regions where large momenta are expected. Numerical results are presented for scattering of Ar-atomic wavepackets from a Cu model surface.

Mikhailova and Pupyshev [65] have improved the accuracy of the *symmetric expansions* for the TDSE evolution *operator up to the fifth order* in time. This formula was applied to MBS. It may also be appropriate to apply it to TEAS.

Gollub and Richards [66] implemented a TDSE solver on *parallel computers* by using a space-splitting method [67] without spectral computations. Second-order approximation of a Laplacian resulted in special tridiagonal matrices and their exponential functions have been computed to provide efficient formulations for parallel computers.

A *pseudo-spectral method* for solving the TDSE in *spherical coordinates* was presented by Corey and Lemoine [68]. The translational kinetic energy operator was evaluated by Fourier transformation. The angular dependence of the wavefunction was expanded on a two-dimensional grid in coordinate space and the angular part of the Laplace operator was evaluated using a *Gauss–Legendre–Fourier transform* between the coordinate and the conjugate angular momentum representations. Calculation was performed for a H_2 molecule scattering on a frozen periodic surface.

Lemoine [69] published a numerical algorithm (the so-called *discrete Bessel transform*) and a FORTRAN 77 program for optimal cylindrical and spherical Bessel transforms satisfying bound-state boundary conditions. The illustrative program applies the discrete Bessel transform to the eigenvalue calculation for two- and three-dimensional harmonic oscillators.

4. Computer animation

To exploit CSMs, computer animation of the physical quantities can be a useful tool. An 'animation' consists of consecutive snapshots of the physical quantity, taken as the time elapses. The manner of the animation depends on the space dimension of the physical problem. A 2D problem can be rendered as a series of 3D snapshots. A 3D problem would demand a 4D full graphical demonstration which is impossible. However, one can produce snapshots of 2D slices (the window technique) in the space or snapshots of isosurfaces (the isosurface technique). The window technique might involve 2D rendering using a colour scale to show the distribution of the physical quantity or 3D rendering of 2D surfaces. In the isosurface technique one can find the points in the 3D space where the physical quantities are equivalent to a given value. In the case of the isosurface technique the most important question is how to choose the isosurface value. For the window technique and 3D snapshots, some applications can be found in [70]—namely, to TEAS from 2D and 3D corrugated surfaces near the interaction and in the detector region, reflecting the evolution of diffraction peaks and adsorption. Some 'picturesque' computer animations can be seen in [71].

As research shows, the human–computer interface is important [72]. Advances in computer technology have led to enhanced 'user-friendliness'. Increased richness and consideration of the end-user in interface design have led to computers becoming more helpful in decision making.

Animation techniques might become efficient in the case of inverse procedures, too. Murray-Smith analysed the problem of inverse techniques for dynamic simulation models [73]. These techniques allow computation of the time history of 'inputs' needed to achieve a specified time history for a selected set of 'outputs'. In general terms, the available methods of inverse simulation may be numerical differentiation or iterative techniques. The iterative techniques are based upon numerical integration processes.

5. Atom scattering on surfaces

A relevant question is whether purely quantum mechanical, semiclassical or classical models have to be treated and whether the probe particle–surface coupling is considered or not. The type of model depends on the physical processes and applications. In many cases it is enough to apply a frozen-surface model when the coupling between the probe particle and the solid surface is not of primary interest. This situation might occur in investigating surface structure, surface disorder and adsorption dynamics (see details concerning molecule dynamics in section 6). However, if one wishes to determine or explore the solid-surface dynamics, the coupling of the probe atom to the vibrating surface becomes relevant. In general, if the probe particle energy (or mass) is high enough, classical or semiclassical models are acceptable. This assertion is supported by the following computations. A semiclassical rainbow analysis of He–Cu(115) and Cu(117) is presented in [74]. This is based on a semiclassical approximation to S-matrix summation over all appropriate trajectories. The method of quantum trajectories proposed by de Broglie and Bohm was applied in the study of atom diffraction on surfaces [75]. There is excellent agreement with results calculated by the standard S-matrix methods of scattering theory. The de Broglie and Bohm quantum theory was solved numerically by Heller's [76] method. Heller's approach is based on appropriate wavepacket propagation.

The transition to the classical limit in atom–surface diffraction was studied using the de Broglie–Bohm causal formalism [77]. In order to achieve this limit, the mass of the probe particles was increased in the case of scattering on the Cu(110) surface. Quantum trajectories mimicked the classical intensity distribution.

5.1. Details of computations

The TDSE was solved numerically by the present author [78] using the seven-SPO time-step formula, which is more efficient than the standard three-SPO one. This numerical solution procedure can handle the time-dependent Hamilton operator when the interaction energy and kinetic energy operators can be separated. The TDSE describes the atomic beam as a quantum ensemble of independent particles. Let us consider the 3D TDSE:

$$\mathrm{i}\hbar\frac{\partial\Psi(\boldsymbol{r},t)}{\partial t}=H\Psi(\boldsymbol{r},t),\qquad H=-\frac{\hbar^2}{2m}\left(\frac{\partial^2}{\partial x^2}+\frac{\partial^2}{\partial y^2}+\frac{\partial^2}{\partial z^2}\right)+V(\boldsymbol{r},t). \tag{1}$$

$\hbar$ is the Planck constant divided by 2π, H is the Hamiltonian, (x, y, z) are Cartesian coordinates and $V(\boldsymbol{r}, t)$ is the particle/surface interaction energy. The interaction energy depends on the particle/surface system and it can be obtained by trial and error using a semi-empirical model of the measurements. The initial wavefunctions—which are used in TEAS calculations—are Gaussian-type wavepackets:

$$\Psi(x, y, z, t=0)=C\exp(-(x-x_0)^2/2\sigma_1^2-(y-y_0)^2/2\sigma_2^2-(z-z_0)^2/2\sigma_3^2)\exp(\mathrm{i}\boldsymbol{k}\cdot\boldsymbol{r}). \tag{2}$$

Ψ is the wavefunction, t is the time, C is the normalization constant, (x_0, y_0, z_0) is the average position at $t = 0$, σ is the standard deviation, 'i' is the square root of -1, $\boldsymbol{k}$ is the wavevector

and $\boldsymbol{r}$ is the position vector. The y-coordinate is omitted in two-dimensional calculations; the solid surface is only corrugated in one dimension.

5.2. He diffraction and transfer width

Stern and co-workers demonstrated the wave theory of probe particles, when they first observed diffraction patterns of He atoms and H_2 scattering from LiF and NaCl surfaces [79–81]. The present author performed a computer simulation of the diffraction pattern in the case of He–W(112) model surface scattering and analysed the transfer width as a function of the energy spread of the incoming atomic beam and of the lattice constant [82]. To describe the He–W(112) interaction potential, a 1D corrugated Lennard-Jones–Devonshire-type potential was chosen:

$$V(x,z) = D\exp(-2\alpha z)\left\{1 - 2\beta\left[\cos\left(\frac{2\pi}{a}x\right)\right]\right\}. \tag{3}$$

D is the energy constant, α is the repulsion constant, β is the corrugation constant and a is the lattice constant. The standard deviation of the incoming wavepacket and the period of the surface are changed and the diffraction pattern is computed and visualized. The main data used in the 2D computations are the following (in atomic units (au)): in equation (2): $k_x = 0$, $k_z = -4$; in equation (3): $D = 0.000\,12$, $\alpha = 0.582$, $\beta = 0.2$. The basis of the model calculations is the result that the energy spread is in inverse ratio to the coordinate spread [82]. Figure 1 shows the different stages of the PDFs of the scattering in the momentum space when (in au): $\sigma_1 = \sqrt{5}$, $\sigma_3 = \sqrt{5}$ and $a = 5.18$. Figures 1A and I correspond to the atomic source region and the detector region, respectively. An approximately monoenergetic beam can be seen in figure 1A and clear-cut diffraction peaks are apparent in figure 1I. The PDF of the interaction process is shown in figures 1B–H as a function of time.

If the transfer width is greater than the typical size of the surface period, diffraction peaks appear. Two types of model computation are executed to analyse the connection between the transfer width and the diffraction pattern. Figure 2 shows the case where the period of the surface is constant and the energy spread of the beam is changed; in the order A–D, the monochromaticity of the atomic beam is decreased. The relative velocity spread (RVS) of the initial wavefunction was determined from the Heisenberg inequality. In figures 2A and B there are narrow diffraction patterns which correspond to the supersonic atomic source. The diffraction peaks have greater FWHMs in figure 2C. Figure 2D does not show a structured intensity distribution because the transfer width is less than the period of the surface.

Let us examine figure 3. The period of the surface is changed and the energy spread of the beam is constant. In figure 3A the diffraction peaks are well defined and the clear-cut peaks of the intensity distribution disappear as the lattice constant of the surface is increased significantly. The diffraction peaks overlap each other in figures 3B and C. The resolution of the TEAS is abruptly decreased as the lattice constant is increased. In figure 3D only the specular peak can be seen and it is a narrower peak than in figure 3C.

The above results support the idea that the transfer width has to be significantly greater than the surface period. Otherwise, the resolution of the experiment is not sufficient for determining the exact surface structure.

5.3. He diffraction from clean and stepped surfaces

He scattering from clean and stepped surfaces was investigated in the case of a general model surface and a Rh(311) surface by the present author [78]. The irregularly stepped surface disrupts the intensity distribution as compared to the periodic surface. The deformation characterizes the surface topography. Systematic classification of model computations might

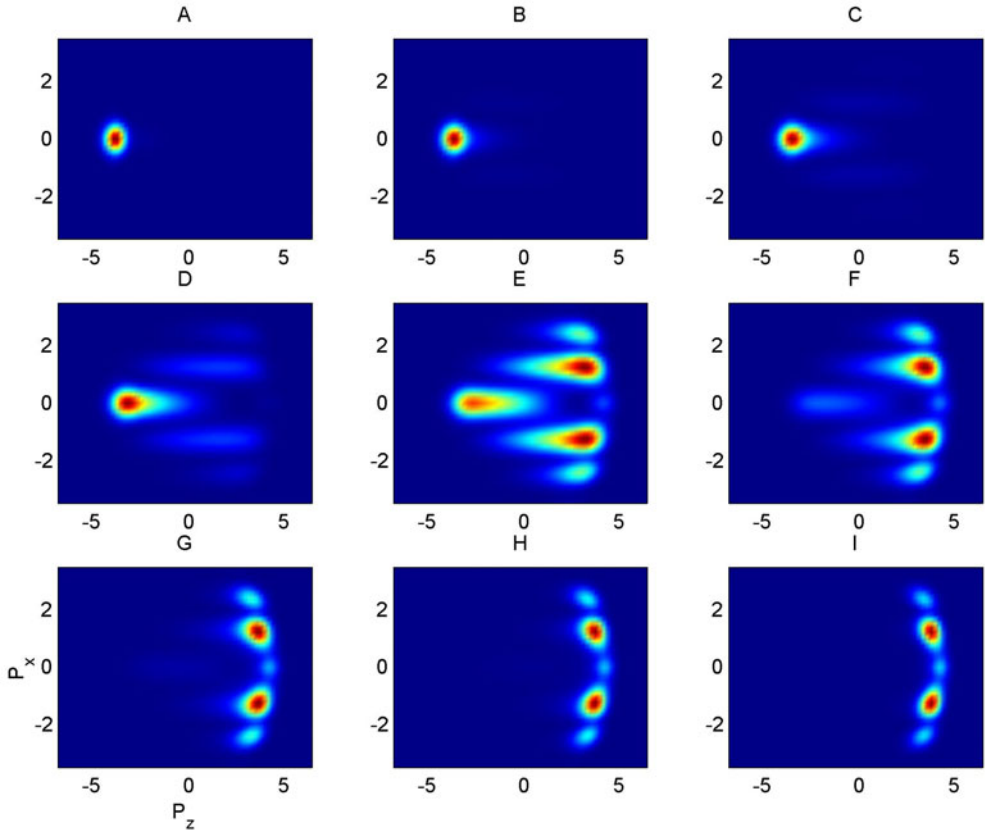

Figure 1. PDFs of He–W(112) scattering propagation in momentum space shown using a colour scale technique. P_x and P_z are the momenta in directions x and z, respectively. Atomic units are used. A: the PDF is in the beam source region (initial state). B–H: the PDF propagates in the interaction region. I: the PDF is in the detector region (final state).

provide a connection to the surface structure and the intensity distribution of the TEAS. Now, let us consider two 3D model calculations and animations of He scattering.

First of all, He scattering on Rh(311) is considered. A corrugated Morse interaction potential describes the Rh(311) surface:

$$V(\boldsymbol{R}, z) = D[\exp(-2\alpha(z - \zeta(\boldsymbol{R}) - \text{disorder}(x, y))) - 2\exp(-\alpha(z - \zeta(\boldsymbol{R}) - \text{disorder}(x, y)))], \tag{4}$$

where $\zeta(\boldsymbol{R})$ is the corrugation function and the position vector $\boldsymbol{R}$ is parallel to the surface [83]. An approximately 63 meV He beam was scattered by regularly stepped Rh(311) surfaces [84]. As is known, the ordered Rh(311) surface is a regularly stepped surface. The input data (au) in equation (2) are: $x_0 = 9.86$, $y_0 = 16.84$, $z_0 \approx 17$, $\sigma_1 = \sigma_2 = \sigma_3 = \sqrt{5}$, $k_x = 0$, $k_y = 4.123$, $k_z = -4.123$. The input data in equation (4) are: $D = 7.74$ meV, $\alpha = 1.01$ Å^{-1}, $\text{disorder}(x, y) = 0$ and the parameters of the corrugation function were chosen from the literature [83]. The corrugation parameters were fitted to the experimental results using the HCW model. Obviously, equation (4) does not provide the effective corrugation function. However, it does provide a good approach to the interaction potential in first order. The angle of incidence of the He beam is 45°. The snapshots of the PDF in real space are rendered as

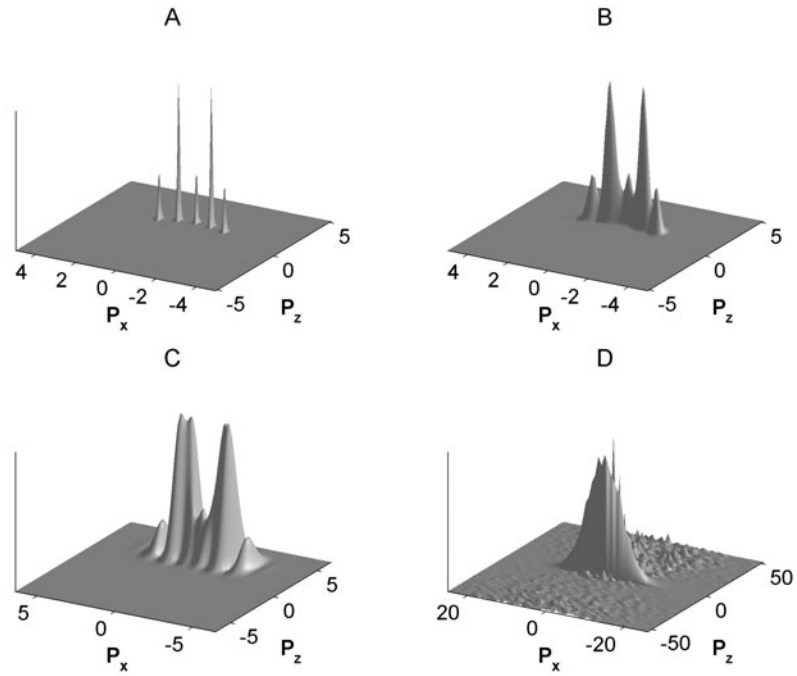

Figure 2. PDFs for different RVSs of the initial wavefunction presented using the 3D rendering technique. P_x and P_z are the momenta in directions x and z, respectively. Atomic units are used. A: the RVS is 0 and 5% in directions x and z, respectively. B: the RVS is 5% in both directions. C: the RVS is 13% in both directions. D: the RVS is 80% in both directions.

a function of time by the *isosurface technique*. The isosurface value is approximately 5% of the maximum of the PDF in the source region. An isosurface of the interaction potential is also shown to allow one to envisage the penetration of the wavepacket into the very top layer of the surface. In the initial state the isosurface is a sphere (figure 4A) because of the input data, but in the detector region a set of diffraction states have evolved containing separate domains (figure 4I). The intermediate states provide information on the scattering dynamics. The interaction is strong in a small region near the surface.

The second example describes the interaction process near the surface—in the quantum mechanical region—*using the window technique* applied to a clean model surface. A Lennard-Jones–Devonshire-type interaction potential has been chosen [78]:

$$V(x, y, z) = D\exp(-2\alpha(z - \text{disorder}(x, y)))\left\{1 - 2\beta\left[\cos\left(\frac{2\pi}{a}x\right) + \cos\left(\frac{2\pi}{a}y\right)\right]\right\}, \qquad (5)$$

where D is the energy constant, α is the repulsive constant, β is the corrugation constant and a is the lattice constant; disorder(x, y) governs the surface disorder.

A completely periodic solid surface was analysed for the case of an approximately 30 meV He beam. (The input data (au) in equation (2) are: $x_0 = y_0 = 18.13$, $z_0 = 16.67$, $\sigma_1 = \sigma_2 = \sigma_3 = \sqrt{5}$, $k_x = k_y = 0$, $k_z = -4$; the input data (au) in equation (5) are: $D = 0.000\,12$, $\alpha = 0.582$, $\beta = 0.2$, $a = 5.18$, disorder$(x, y) = 0$). As is known, the scattering process leads to a diffractive intensity distribution. The most relevant question is what happens near the surface in the quantum region. To answer this question, parallel slices of the PDF of the He atoms scattered to the solid surface have been obtained as time elapsed near the classical turning

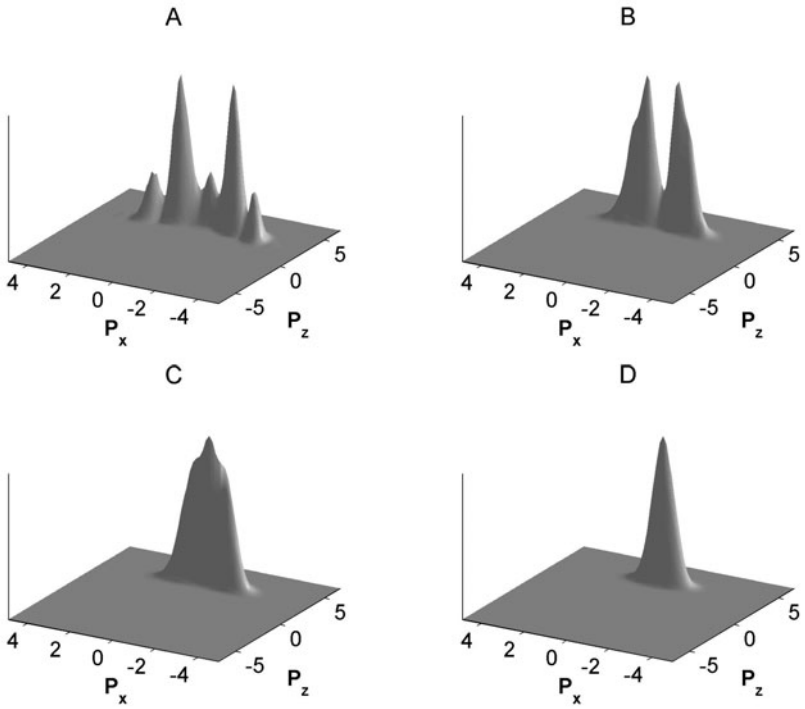

Figure 3. PDFs for different lattice constants presented using the 3D rendering technique. P_x and P_z are the momenta in directions x and z, respectively. The RVS of initial wavefunction is 5% in both directions. A: the lattice constant is 5.18 au. B: the lattice constant is 10 au. C: the lattice constant is 13 au. D: the lattice constant is 20 au. Atomic units are used.

point. The PDF can be obtained as the square of the absolute value of the wavefunction; the wavefunction is calculated by the TDWP method. In figure 5 one can see colour scale snapshots of the PDF in the momentum space as a function of time. First, the wavepacket is approaching the surface—towards the window parallel to the surface, where we obtain the slices of the PDF. Figure 5A only shows a small and dim spot. The wavepacket, however, is going towards the surface and the window slice of the PDF becomes larger and more complicated. The bright spots correspond to the diffraction channel. In the interaction region, close channels also appeared, which were evanescent during the scattering. For example, in figures 5F and G one can see the two-dimensional Brillouin zones in the order first, second, third relating to a square lattice. After the interaction, the wavepacket leaves the surface behind and the window slice becomes dim and empty again (figure 5I).

A further effect is the step-edge orientation, which should be discussed using the TDWP method. Helium-atom scattering has been used to determine the step-edge orientation on a Rh(311) surface, whose close-packed rows are separated by alternating (100) and (111) microfacets [85]. Additional peaks were observed from the specular beam when the incident He beam impinged on the (100) or (111) microfacets. The stepped surface structure can be investigated using this effect.

An another new problem occurred upon exposing the He beam at a grazing angle. Diffraction beams from the scattering of He atoms from the Rh(311) surface were observed at scattering angles of up to grazing exit, at nearly 90° with respect to the surface normal [86]. Under grazing exit conditions, a broad scattered signal appears which is interpreted as diffuse

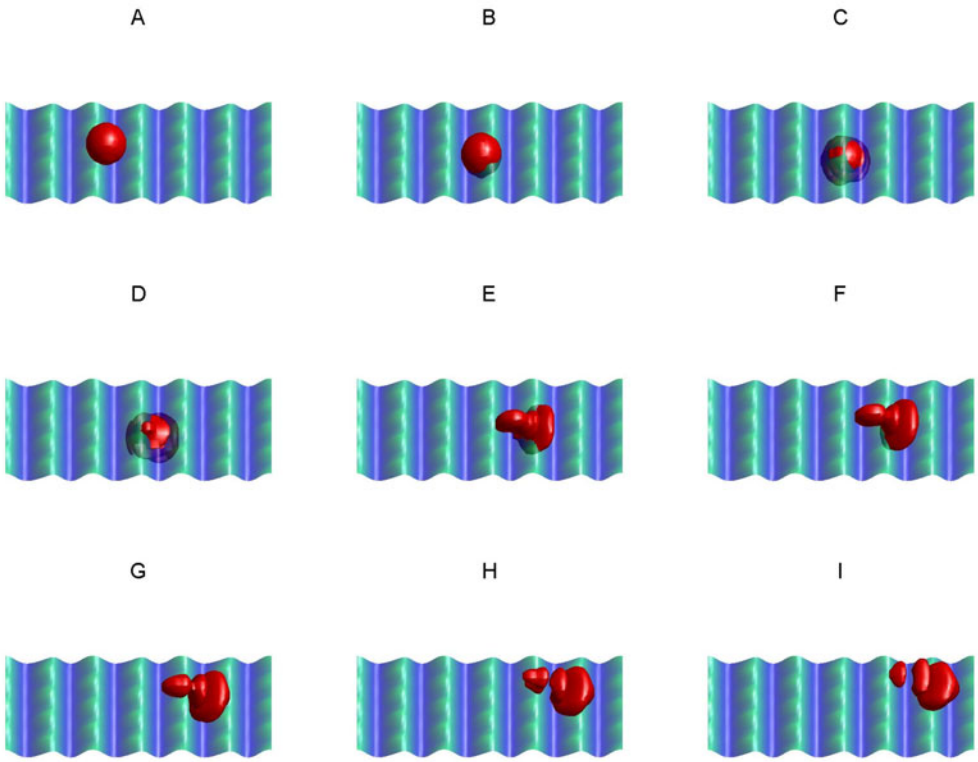

Figure 4. 'Animation' by the isosurface technique in real space. The isosurface value is approximately 5% of the maximum of the PDF at the initial time. The isosurfaces of the PDF are rendered as a function of time in the order ABC. A: the initial wavefunction. B–H: the interaction region. I: the final state. An isosurface of the interaction potential is also shown.

scattering of the grazing diffraction beam arising from collisions with the low-density step defects resulting from the small miscut of the crystal. This experiment opens new possibilities for the characterization of surface defects with diffraction techniques. However, in the 'upstairs' and 'downstairs' directions there are significant differences between the intensities in the (01) direction. This phenomenon is explained not by a close-coupling calculation but by the Fraunhoffer diffraction model. The TDWP method is able to determine which direction is 'uphill'. The TDWP method, however, demands a long region parallel to the surface in the azimuth angle direction as well as an absorbing boundary, because of the grazing angle.

5.4. He scattering on adsorbed surfaces

TEAS can be used to determine the surface topography by exploiting the intensity distribution. The diffraction beam becomes very clear-cut when the surface structure is periodic again. Exposing the surface top layer to an adsorbate beam, a periodic superlattice can be developed relating to the adsorbate coverage rate and the adsorbate structure. The details of this topic are reviewed in [11]. However, let us examine some experiments, since these are necessary for the further discussion and provide experimental results for comparison with the theoretical TDWP calculations.

The (311) surfaces of fcc materials are of special interest as they offer a large variety of differently coordinated adsorption sites [87]. Rh(311) was obtained by He diffraction.

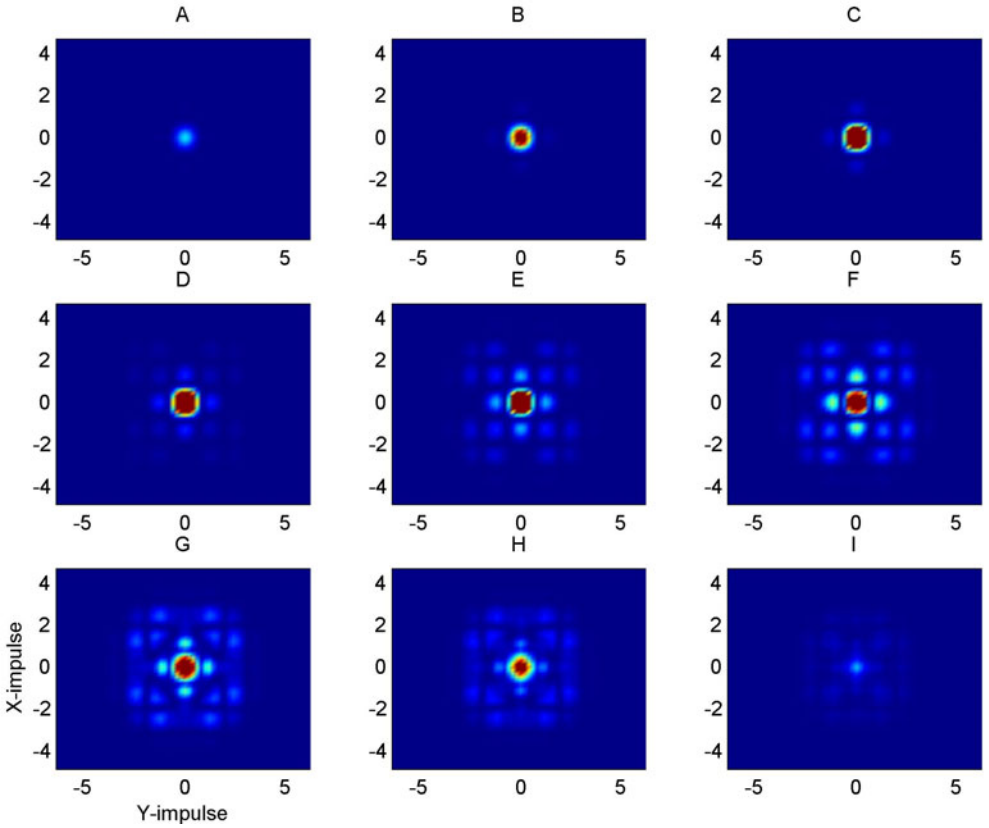

Figure 5. 'Animation' by the window technique using a colour scale in momentum space. Slices of the PDF parallel to the periodic surface—near the interaction region as time progresses—are rendered. P_x and P_y are momenta in the directions x and y, respectively. A: the wavepacket has just reached the window. B–H: the wavepacket is in the interaction region. I: the wavepacket has just left the window behind. Atomic units are used.

Development of hydrogen phases on Rh(311) was achieved by hydrogen exposure. The sequence of the superstructures in order of increasing exposure is as follows: c(1 × 1)H, c(1 × 3), p(1 × 1)H and p(1 × 1)H (REC).

The adsorption of oxygen on Rh(311) has been investigated by means of He scattering [88]. The formation of ordered (2 × 1) and (1 × 3) structures was observed. The experimental results suggest that oxygen induces a surface reconstruction in the (1 × 3) phase, wherein at least one of the three close-packed rows is missing and the oxygen atoms fill the resulting deep troughs.

The formation of ordered structures of hydrogen on Pd(311) has been investigated using low-temperature He beams [89]. Before completion of a saturated c(1 × 1) phase, formation of three low-coverage (2 × 1) phases was found. Possible structural models for the reported phases have also been discussed [89].

The formation of ordered oxygen overlayers on Pd(311) as well as structures obtained after their reduction in hydrogen have been studied by means of He scattering [90]. The presence of a pronounced rainbow pattern in the (1 × 2) in-plane spectra shows unambiguously that its structure is of missing-row type. Possible structural models for different phases were recommended.

Low-energy vibrations of CO adsorbed on Ni(110) were investigated carefully using high-resolution He-atom scattering [139].

The above and other experiments have been discussed in detail [11], but further investigation using the TDWP method might provide additional elaboration of the intensity distribution, as is seen below.

Helium-atom scattering is suitable for use in characterizing the correct orientation in a (1×1) CO commensurate monolayer adsorbed on a single crystal NaCl(100) surface; this was investigated in [91]. The fully quantum mechanical description is based on two potentials which exhibit a significant discrepancy according to whether the CO axis is normal to the surface or inclined at about 40°. The computation results indicated that He diffraction can be used to determine the structure of the (1×1) CO phase. The TDWP method used to compute the diffraction spectra was the same as in Lemoine's paper [92], apart from a special splitting algorithm [93]. The wavefunction for the scattering is expanded in terms of plane waves for the two-dimensional reciprocal space. In the case of off-normal He incidence, the diffractive scattering symmetry was exploited [92]. The computed intensity distributions of two different CO phase positions show a significant discrepancy. In the wavepacket picture the trapped portion is slowly leaking out of the interaction into the asymptotic region. Even if one finally turns the grid as the wavefunction spreads, the multi-dimensional computation may be too large. This problem can be resolved by using a complex absorbing potential or splitting the outgoing packets into an interaction part and an asymptotic part [93]. This splitting procedure should be repeated until the intensity of the wavefunction becomes negligible in the interaction region. Both the interaction and asymptotic pieces have to be back-transformed to momentum space, either for the propagation step or for the final asymptotic analyses. The splitting operator method has to avoid the discontinuities.

A numerically exact TDWP quantum calculation of the He scattering from single CO adsorbates on Pt(111) has been demonstrated that is based on a soft potential closely approximating the hemisphere geometry [94]. The model calculations showed good agreement with experimental angular distribution.

5.5. He resonant adsorption on a Rh(311) surface

On the basis of a TDWP method calculation and assuming an exponential decay law for the resonances, Hernández *et al* [95] computed the selective-adsorption resonances in the elastic scattering of He atoms from the Cu(110) and Cu(117) surfaces.

Miret-Artés [96] proposed a systematic classification of the elementary processes within the close-coupling formalism. The term 'elementary' means that the entrance scattering channel directly leads to the formation of the resonance without intermediate states and the single-phonon approximation holds. Fourteen different cases were discussed. Also, theoretically predicted and experimentally observed mechanisms were described. The multi-phonon contributions to the elastic diffracted intensities and resonance profiles were considered in [97] for scattering of He atoms from the surfaces Cu(110) and Cu(113).

Diffraction studies were performed with He and Ne beams on clean Rh(311) and c(1×1)H phases [83]. Selective adsorption of He on clean Rh(311) and c(1×1)H phases was measured, allowing the determination of three and four bound-state levels, respectively. These parameters were fitted to a two-parameter Morse potential.

Let us investigate the resonant adsorption of the He–Rh(311) system with the TDWP method [111]. This system is the same as that in section 5.3 and the numerical procedure is similar to the one applied there. In equation (2) the main input parameters for the He beam are (in au): $\sigma = \sqrt{5}$, $x_0 = 9.8644$, $y_0 = 12.681$, $z_0 = 11$ and $\boldsymbol{k} = (k_x = 0, k_y =$

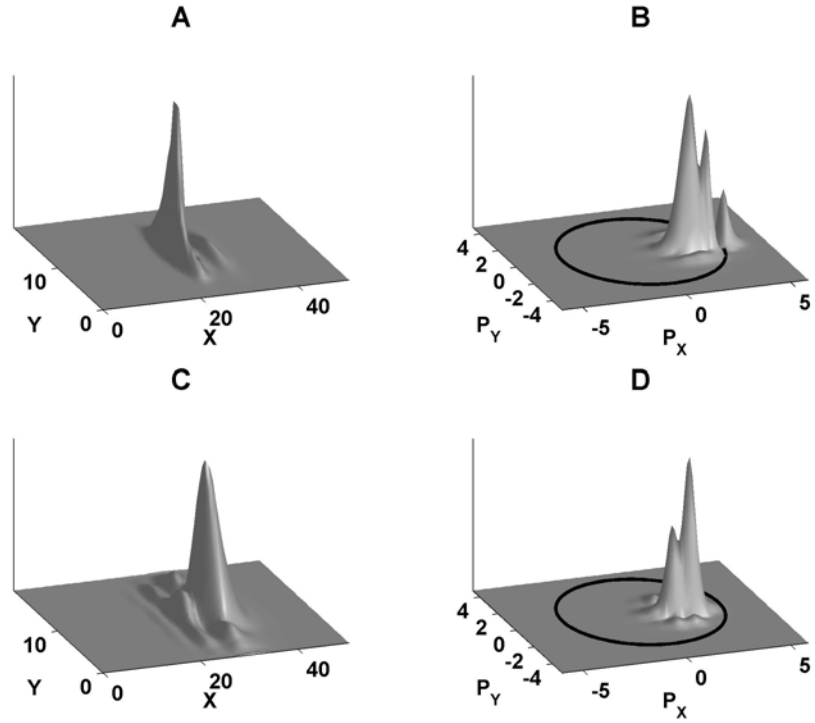

Figure 6. He resonant adsorption on He–Rh(311): scattering investigated by the window technique with 3D rendering. Atomic units are used. The PDF is split into slices parallel to the solid surface. P_x and P_y are the momenta in the directions x and y, respectively. A and B: the PDFs are shown in the real space and in the momentum space, respectively, when the wavepacket is near the classical turning point ($\langle z\rangle = 2.62$ au, $z = 2.62$). The radius of the circle at the origin is 3.74 (au). C and D: the PDFs are shown in the real and the momentum space when the wavepacket is in the detector region. The radius of the circle at the origin is 3.74 (au).

3.0636, $k_z = -2.1452$), $k = 3.74$. The average energy of the He atom is: ≈26 meV. The incident angle is: $\Theta_i = 55^\circ$. 32, 96 and 64 sample points are chosen in the directions x, y and z, respectively. In figures 6A and B the PDFs are shown in the real and in the momentum space, respectively, as the wavepacket approaches the classical turning point ($\langle z\rangle = 2.62$ au, where '$\langle\ \rangle$' stands for the average). The PDF is equal to $|\Psi(\boldsymbol{r}, t)|^2$. The PDF is split into slices parallel to the solid surface, since it is a function of three variables in space. In this region the He–surface interaction is crucial. A very important fact is clear: for $|\boldsymbol{k}| > 3.74$ au, the probability significantly differs from zero. This corresponds to the bound states, because the perpendicular motion is limited, so a fraction of the He atoms have longer lifetimes near the Rh(311) surface. Figures 6C and D show the PDF after the scattering, beyond the interaction region, in the real and in the momentum space. One can also see in-plane and out-of-plane scattering. The component of the wavevector $\boldsymbol{k}$ parallel to the surface is shorter than 3.74 au, however, when the He atom is near the top layer of the Rh(311) surface. The attractive part of the interaction potential leads to longer lifetimes near the surface.

5.6. Classical and quantum chaos

Recently some classical and semiclassical calculations of atom scattering showed chaotic effects. Guantes *et al* [98] discovered classical chaos of the He scattering on Cu(117) relating to right-angle rainbow scattering. The scattering phenomenon becomes extremely sensitive to the scattering parameter. This yields the fractal structure of the curve of the He-atom deflection angle (the impact parameter) [99].

Miret-Artés *et al* showed that the diffraction condition for the scattering of atoms from surfaces leads to the appearance of a distinct type of classical singularity [100]. It is also shown that the onset of classical trapping and chaos is closely related to the bifurcation-order function around the surface points showing the rainbow effect. The scattering of He atoms on stepped Cu(115) is discussed.

Guantes *et al* [101] investigated the phase diagrams (e.g. periodic orbits and homoclinic tangle) for He-atom scattering on a Cu surface, considering the chaotic scattering within the framework of the classical theory.

A classical picture of threshold resonances in classical chaotic surface scattering was explored [102]. It was also emphasized that these resonances are observable for highly corrugated surfaces or for smooth surfaces with incidence conditions where multiple scattering is important.

Semiclassical *S*-matrix theory was applied in the case of classically chaotic scattering [103]. According to the basic assumption, the direct and complex contributions to the *S*-matrix can be computed independently. Only the interference among trajectories corresponding to the same 'icicle' was considered. If a chattering region (irregular curve) is expanded, a series of smooth subdomains—called 'icicles'—can be found. This is equivalent to assuming that the interferences between all trajectories in different icicles will cancel each other, on average.

Hernández *et al* [104] investigated the time evolution of He scattering on Cu(110) using a time-dependent autocorrelation function for a wavepacket. The wavepacket time propagation was determined by solving the TDSE using a finite-difference scheme. All memory of the initial wavepacket was rapidly lost. The same results were obtained by a method of halfwidth analysis.

Classical models of scattering techniques often show chaotic behaviour. This raises the question of quantum chaos. The intensities of low-energy electron diffraction and photoelectron diffraction (PED) are analysed from a statistical point of view in [105]. To characterize chaotic wavefunctions, Porter and Thomas [106] advanced the hypothesis that *wavefunctions of a chaotic system should display a* χ^2_ν*-type statistical probability distribution*. This hypothesis has been rigorously justified using supersymmetry formalism [107] and has been used as a convenient definition of quantum chaos. This hypothesis can at least be thought of as a necessary condition. Dyson [108] demonstrated that within the random-matrix theory [109], only three universal classes exist. Depending on whether the Hamilton operator is constructed with real numbers, complex numbers or quaternions, ν is one, two or four degrees of freedom, respectively.

A good understanding of wavefunctions is crucial in explaining open systems—namely the probe–target–probe set-up that is used in most scattering arrangements. In the case of quantum scattering phenomena, the number of degrees of freedom is 2, because the wavefunctions are complex functions. The calculations by de Andres and Vergés [105, 110] proved that the intensity distribution of the low-energy electron diffraction (LEED) and the PED fit quite well to the χ^2_2-type statistical distribution. The most complex models of LEED and PED fit to the χ^2_2-type statistical distribution best. These systems exhibit quantum chaos in the case of scattering on ordered surfaces, which is a remarkable result.

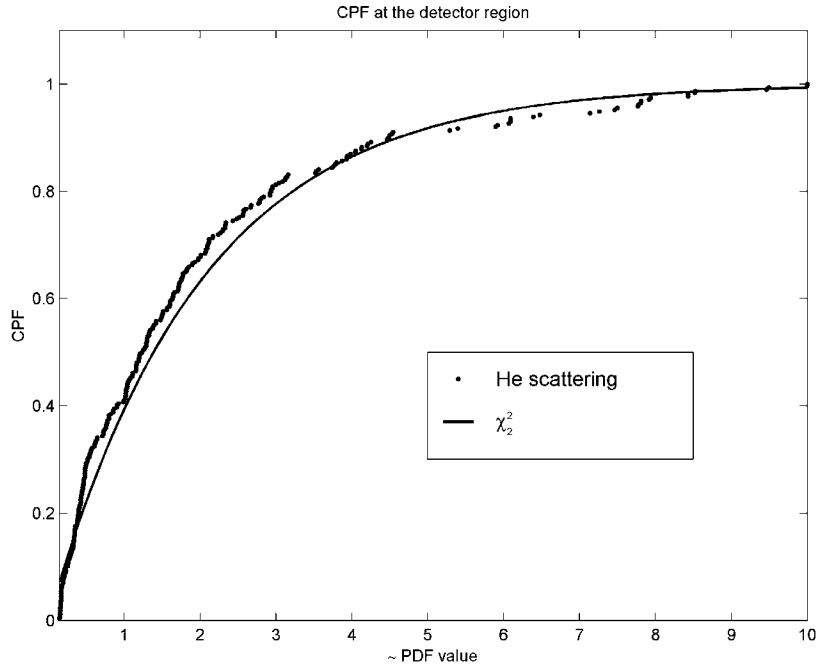

Figure 7. The CPF for the He PDF in the case of He scattering on a W(112) model surface. The thick solid curve shows the theoretical χ^2_2-law. Filled dots show the CPF from TDWP model calculations in the detector region after the scattering process. The PDF is equal to $|\Psi(\boldsymbol{r}, t)|^2$, where $\boldsymbol{r}$ is the position and t is the time.

5.6.1. Manifestation of quantum chaos in TEAS. The present author was inspired to investigate the quantum chaos of TEAS on the basis of section 5.6. Recently, Balázs *et al* discovered the chaotic effect of the three-dimensional He–Rh(311) system [111]. However, the search for quantum chaos was unsuccessful. The dwell time of the He atom—in a chosen volume—was the physical quantity that should have shown stochastic behaviour. Now, I analysed the diffraction pattern of He–W(112) model surface [82] in the detector region. The PDF was determined by the TDWP method for absolutely the same system as was discussed in section 5.2 and shown in figure 1. Figure 7 shows quite good agreement between the calculated scattering cumulative probability function (CPF) of the PDF and the χ^2_2-law. *This preliminary result manifests the quantum chaos of He–W(112) model surface scattering—albeit that a well ordered system was dissected.* This corresponds to the quantum chaotic behaviour of LEED and PED. The elaboration of the quantum chaos in the case of TEAS will be published elsewhere.

5.7. Scattering from vibrating surfaces

A very detailed review can be found in [12] devoted to single- and multi-phonon processes of TEAS. The projectile particle colliding with a surface may exchange zero, one or more quanta with the phonon heat bath. Consequently there is non-zero probability of elastic scattering; this circumstance demands scattering boundary conditions on the perturbing potentials of phonon processes [112]. Under certain conditions the motion of probe particles and surface vibrations can be treated by classical mechanics. This is likely to be the case for large masses of probe particle and surface atoms and high projectile incident energy [113]. Several semiclassical schemes and approximations have been developed. For example, the probe

particle translational degrees of freedom are treated classically or semiclassically (heavy probe particles) and surface vibrational degrees of freedom quantum mechanically. In another case the light probe particle is treated within quantum mechanics and surface degrees of freedom classically. The classical treatment of surface vibrations is usually based on a description by the generalized Langevin equation [114]. A quantum treatment of light-atom–surface inelastic scattering proves indispensable under scattering conditions typical of TEAS [115, 116]. Standard quantum mechanical theory of scattering is well established [117, 118]. The applicability of the previously mentioned approaches depends on the scattering regime (classical, semiclassical or quantum) in which the experiments have been carried out. An unified theory of He scattering of thermal energy should contain the quantum formalism, unitarity in the sum of all scattering probabilities, full surface vibrational dynamics, the limit in the one-phonon scattering regime and quantum treatment of multi-phonon scattering in three dimensions. The scattering spectrum approach (SSA) model wants to fulfil the condition of unification [119]. Different developments can be found in [120–123]—calculations of the Debye–Waller factors, Born approximations and He energy transfer to surfaces.

One can see how complicated the question of the coupling between the probe particle and the solid surface is. The advantage of the TDWP approach is that the surface may contain arbitrary disorders and the atomic beam may be non-monoenergetic. The disadvantage of the TDWP approach is the limited number of degrees of freedom in consequence of the high computer effort requirements. If one wants to exploit the quantum description of the TDWP, then three degrees of freedom are occupied for translational motion of the probe atom. A classical coupling can be provided with a classical discussion of solid-surface vibration via the generalized Langevin equation [114]. The surface consists of two zones. In the first zone there are the target atoms, which directly collide with probe atoms. The second zone contains the surface atoms, which experience the interaction with the probe atom described via the so-called memory function. This model should contain ordinary coupled differential equations for surface atoms. These equations are related to the TDSE and vice versa. The coupling is attained via the energy of interaction between the scattering atom and the pairwise surface potential. If the scattering atom does not influence the surface atoms, the approximation corresponds to a purely thermally vibrating system without any energy change. This is the simple kinematic theory [70]. Details of the TDWP method using the Langevin equation will be published elsewhere.

6. Molecule scattering on solid surfaces

A fruitful application of the TDWP method is in the investigation of reactions at surfaces [124,125]. Understanding reactions at surfaces plays an important role in understanding: heterogeneous catalysis, crystal growth determining the quality of semiconductor devices; corrosion and lubrication, influencing the durability of mechanical systems; hydrogen storage in metals; and so on. In the last decade the increase in computer power and the development of *ab initio* surface calculations has led to the fully quantum mechanical dynamics calculation of scattering of diatomic molecules (mainly H_2) from solid surfaces. So-called *ab initio* dynamics calculations of reactions on surfaces usually require three independent steps:

- determination of an *ab initio* PES by first-principles total-energy calculations;
- a fit of the total energies to an analytical or numerical continuous representation which serves as an interpolation between the actual calculated points;
- a dynamical calculation on this representation of the *ab initio* PES that includes all relevant degrees of freedom.

6.1. Theoretical background of molecule/surface dynamics

To take into account fully quantum mechanical calculations to analyse the dynamics of molecule–surface interaction some relevant theoretical approximations are necessary. A detailed description can be found in [125, 126]. A short description of molecule–surface dynamics based on the papers [125, 126] can be read below.

One common approach is to assume that—due to the large mass difference between electrons and the nucleus—the electrons follow the motion of the nucleus adiabatically. This is the *Born–Oppenheimer approximation* [127]. In gas–surface scattering, electronically non-adiabatic processes are indeed occurring. However, the proper treatment of non-adiabatic processes is rather complex. Solving the Schrödinger equation here is too complex, since the phonons have an infinite number of degrees of freedom.

One additional approximation is considering surface atoms to be frozen at their ideal-lattice positions, thereby allowing *neglect of the phonons*. This model can be handled fully quantum mechanically in the case of diatomic molecules, as we discuss below. The reaction probability curve is characterized by three parameters: the maximum reaction probability, the width parameter and the dynamical barrier height. The mere presence of phonons at zero surface temperature may have an effect on the computed reaction probability, which can only be assessed in theoretical calculations. The reaction probability may be affected by alterations in surface temperature in experiments as well as calculations. In several cases, the maximum probability and the dynamical barrier height are independent of surface temperature. This means that the frozen-surface approximation determines the dynamical height barrier within a few hundredths of an electron volt. The effect of surface temperature may be taken into account by readjusting the width parameter of the reaction probability curve to the surface temperature. For non-activated reactions, the reaction probability is always large and we would expect the surface temperature to be even less important for these reactions.

The calculation of the PES is based on *density functional theory* (DFT) [128, 129]. One serious problem arises from the use of *ab initio* potential energies, in particular in quantum dynamics simulations. To solve the Schrödinger equation, one needs in general a continuous description of the potential, since the wavefunctions are delocalized. The *ab initio* calculations provide total energies for discrete configurations of the nuclei. In order to obtain a continuous description, the *ab initio* energies have to be fitted to an analytical or numerical continuous representation of the PES.

Finally, the Hamilton operator of the diatomic MBS on a rigid solid surface is

$$H_{6D} = -\frac{\hbar^2}{2M}\nabla_{\boldsymbol{R}}^2 - \frac{\hbar^2}{2m}\nabla_r^2 + V_{6D}(\boldsymbol{R}, \boldsymbol{r}),$$

where $\boldsymbol{R}(x, y, z)$ is the vector of the molecule centre of mass. (x, y) is parallel and z perpendicular to the surface. M is the molecule mass and m is the reduced mass of the molecule ($m = (m_1 m_2/(m_1 + m_2))$). Furthermore, $\boldsymbol{r}$ is the vector of the internal coordinates of the molecule, which are usually taken as (r, Θ, Φ). r is the distance of atoms of the molecule, Θ is the polar and Φ is the azimuthal angle of orientation of the molecular axis.

We have two different basic ways to determine the wavefunction. The first way is solution of the TISE; the second is solution of the TDSE. The 6D dynamical problem has been formulated using the CC method, i.e., by writing the TISE as a set of coupled ordinary differential equations instead of a partial differential equation in a scattering coordinate system [126]. The goal is to obtain the scattering S-matrix by the CC method, which corresponds to elastic or inelastic scattering. Since the PES is conservative, the total energy of the probe particle is constant throughout the whole process. However, there are open channels between the different states, e.g., the vibrational and the rotational states. The vibrational or rotational energy may change

and we speak—in this sense—of inelastic scattering. Solution of the TDSE by the TDWP method was discussed in previous sections. For problems involving small scattering basis sets, the computational effort required by the CC method may be comparable with the computational effort required by the TDWP method [130, 131]. However, on involving a bigger scattering basis set, the TDWP calculations become less expensive. The TDWP method will be the most efficient, if the goal is to obtain results for one initial state, but for a large range of energies. The CC method demand for computer memory is much smaller than that of the TDWP method.

Typical quantum numbers are as follows: reciprocal-lattice vector coordinates (m, n); the diffraction quantum numbers; vibrational quantum numbers (v); rotational (angular) quantum numbers (j); and magnetic rotational quantum numbers (m_j). The diffraction quantum numbers relate to the periodic solid surface. It is worth describing the rotational state $|jm_j\rangle$ by means of spherical harmonic functions and the vibration by means of a rovibrational state $|vj\rangle$. The effect of alignment (m_j) on the reaction is important, particularly for two special positions: the $m_j = 0$ 'cartwheel' state and the $m_j = j$ 'helicopter' state. The cartwheel state rotates in a plane perpendicular to the surface, the helicopter state in a plane which is approximately parallel to the surface, m_j being the projection of j on the surface normal.

Investigating the molecule scattering using the above-described model, the diffraction probability and the sticking probability can be computed, too. The sticking may yield dissociative adsorption. The final states show an appropriate distribution of possible quantum states. This implies the evolution of different rovibrational, rotational and translational final states. Experiments and theoretical calculations led to a better understanding of the molecule/surface dynamics. For example, the *steering effect* was underestimated hitherto. A qualitative explanation of the steering effect is as follows. Let us imagine a classical trajectory model and let the molecule position be perpendicular to the surface at a perpendicular incident angle. In the initial state, the molecule can be found in a plane that is perpendicular to the surface. This is a special type of cartwheel position. If the initial kinetic energy is low enough, then the molecule has enough dwell time to be reoriented approximately parallel to the surface. This position means a much higher probability of dissociative adsorption. If the kinetic energy is high enough, the molecule moves so fast that it hits the repulsive wall of the potential before it is in a favourable configuration for dissociative adsorption. The molecule is scattered back into the gas phase rotationally excited.

6.2. Applications of molecular beam scattering

Finally, we mention some results derived from TDWP and CC methods and experiments concerning molecule/surface dynamics. Molecular beam experiments have simultaneously measured not only the diffraction peaks but also the rotational state of H_2 scattered from the surface, and observed rotationally inelastic diffraction, e.g., for Ag(111) [132], Rh(110) [133], Ni(110) [134], Cu(001) [135, 136], LiFl(001) [137, 138]. Elastic rotationally mediated critical kinematic selective adsorption (RMCK-SA) was studied experimentally by scattering D molecules from the Cu(001) surface [140, 141]. In a series of diffraction spectra taken for different surface temperatures between 40 and 500 K, resonance lineshapes were observed. The RMCK-SA effect results from the interaction among several diffraction and rotational channels. From the best fit of the experimental profiles a lifetime for the third bound state of the D-molecule–Cu interaction potential is obtained.

Dai and Light [142] presented a six-dimensional quantum wavepacket dynamics calculation for dissociative adsorption of the H molecule on a Cu(111) surface. The energy surface was taken into account by means of *ab initio* calculations [143]. The dissociation probability with different quantum numbers was determined for all degrees of freedom: namely the three Cartesian coordinates of the centre of mass and three internal coordinates.

Diño *et al* [144] investigated the dissociative adsorption dynamics of a D molecule on a Cu(111) surface using the CC method. To explain the experimental observations, it is necessary to consider the coupling between the rotational degree of freedom of the impinging molecule and the vibrational degree of freedom of the surface.

Harris *et al* [145] compared a mixed quantum–classical treatment of molecule–surface scattering and dissociation dynamics with classical and exact quantum methods. They found that the accuracy of the semi-quantal method is at best as good as that of the classical one, while the computational performance is considerably poorer.

The quantum dynamics has been solved by wavepacket techniques in the case of H_2 scattering [146, 147]. To prevent reflections from the ends of the grid, grid-cutting techniques were used [93, 148].

McCormack and Kroes [149] executed a direct comparison between classical/quasiclassical trajectory results and the six-dimensional quantum wavepacket method in the case of adsorption of a H molecule on a Cu(100) surface. The quasiclassical reaction probability is in much better agreement with the quantum probability than the classical one.

Hydrogen-molecule adsorption on Pd(100) is determined in [150] by *ab initio* quantum and CC molecular dynamics calculations. It is shown that the determination of the PES combined with high-dimensional dynamical calculations leads to a thorough understanding of the hydrogen dissociation dynamics at a transition metal surface. All relevant degrees of freedom are taken into account.

Miura *et al* [151] investigated how the coupling between molecular vibration and rotation affects the direct scattering of H_2 from Cu(111), by performing CC computations. The conclusion is that the rotational excitation in vibrationally elastic scattering processes occurs more preferentially for H_2 in the vibrational excited state than for H_2 in the vibrational ground state in the low-translational-energy region, because the decrease of vibrational energy in the transition-state region is larger for the excited state than for the ground state.

How orientation influences the H_2 dissociative dynamics at different sites along the $Cu_3Pt(111)$ surface lateral direction, where Cu and Pt alternate, is studied in [152]. Computational results show a strong dependence of H_2 dissociation on the H_2 orientation across the Cu–Pt bridge site.

Miura *et al* [153] inquired into the isotope effect on the rotationally inelastic diffraction dynamics of hydrogen scattered from Cu(001), by carrying out CC calculations. A strong isotope effect has been observed; namely, in the low-incident-energy region, the rotationally inelastic diffraction probabilities for D molecules are larger than those for H molecules. On increasing the incident energies, however, the rotationally inelastic diffraction probabilities become smaller than in the case of H molecule.

Miura *et al* [154] investigated the effect of the correlation between molecular diffraction and rotational excitation on the dynamics of H_2 scattering from Cu(001). Apart from some oscillatory structures, rotationally probabilities show opposite incident energy dependences for H_2 doing cartwheel-like rotations (an increase with increasing incident energies) and helicopter-like rotations (a decrease with increasing incident energies).

A time-dependent quantum mechanical study of the *chemisorption* dynamics of H_2 scattering on W(001) is presented in [155]. Bejan *et al* [156] have investigated the *desorption* of CO on Cu surfaces that is induced by hot electrons. The results of the wavepacket computations are in fair agreement with the experimental findings.

Eley–Rideal (ER) reactions between H atoms on metal and graphite surfaces were investigated [157]. In an ER reaction, a gas-phase particle incident on a substrate combines with a particle adsorbed onto that substrate, in contrast to what happens in a Langmuir–Hinshelwood reaction involving diffusing reactant atoms. The TDWP method applied to the ER reactive

scattering between a gas-phase atom and an adsorbate is discussed, in general, in [158]. That paper contains the description of a computer program that handles the ER-problem-solving TDWP method in three dimensions.

Six-dimensional quantum and classical dynamics computations of H_2 scattering on Pt(111) are presented in [159]. The quantum calculation results are in good agreement with recent molecular beam experiments. The quasiclassical method works better than the classical method, the quasiclassical results being in excellent agreement with the quantum results. The physical model consists of making a Born–Oppenheimer approximation and the reaction takes place on the ground-state PES. The Pt surface is frozen; Pt atoms are in equilibrium positions. The remaining six degrees of freedom are treated without further physical approximation. The most expensive calculation contains 168.5 million grid points in the six-dimensional discretized physical space. This quantum computation is a typical TDWP method.

The feasibility of utilizing hydrogen molecules to probe adsorbate–surface interaction, the surface structure and the effective PES for the reaction considered are explored in [160]. From the calculations and according to the experiments with $H_2/Cu_3Pt(111)[1\bar{2}1]$, $H_2/NiAl(110)[1\bar{1}0]$, $H_2/Cu(001)[100]$, it appears that the scattering of H_2 can be used to distinguish between various components on surfaces.

7. Conclusions

The TDWP method has been reviewed, emphasizing its recent applications, numerical solutions and computer animation techniques. Reactive scattering of atom and molecules, atomic and nuclear phenomena in laser fields, electron scattering from molecules, photodissociation, photoabsorption, non-adiabatic processes of molecules, Rutherford scattering, electrons in nanoscale devices, cooling and trapping in quantum wires and dots, STM, TEAS and MBS are recent application areas for the TDWP method, which are involved in present work focusing especially on TEAS and MBS. Among other things, quantum chaotic behaviour of TEAS from an ordered surface has been demonstrated for the first time. The long list of applications supports the importance of the TDWP method. The relevance of the TDWP method has motivated the progression in the numerical procedures and the simulation methods (e.g. animation techniques). The animation techniques might lead to a more accurate understanding of the physical processes. Further research might discuss more complicated atom/molecule–surface interactions: e.g. recording step-edge orientation by means of TEAS; grazing angle TEAS; quantum chaos of TEAS from ordered and disordered surfaces; and molecular dynamics of polyatomic molecules relating to frozen or vibrating surfaces.

Acknowledgment

The research was supported by the Hungarian Scientific Research Fund (T038158).

Appendix

The determination of some physical quantities from the wavefunction has been described without a complete explanation.

The notation system is as follows: Ψ is the state function, $\boldsymbol{r}$ is the position vector, t is the time, F is the operator for a physical quantity, $\boldsymbol{k}$ is the momentum vector, m is the particle mass, i is the square root of -1 and an asterisk indicates a conjugate.

- The average of a physical quantity is $\int_V \Psi^*(\boldsymbol{r},t) F \Psi(\boldsymbol{r},t)\,\mathrm{d}V$, where V is the whole space.
- The PDF in real space is PDFR $= \Psi^*(\boldsymbol{r},t)\Psi(\boldsymbol{r},t)$.
- The PDF in momentum space is PDFM $= \tilde{\Psi}^*(\boldsymbol{k},t)\tilde{\Psi}(\boldsymbol{k},t)$.
- The probability current density is $\boldsymbol{j} = \frac{\hbar}{2mi}[\Psi(\boldsymbol{r},t)^* \nabla\Psi(\boldsymbol{r},t) - (\nabla\Psi(\boldsymbol{r},t)^*)\,\Psi(\boldsymbol{r},t)]$.
- The probability current to a surface is $I = \int_A \boldsymbol{j}\,\mathrm{d}\boldsymbol{A}$.
- The dwell time probability $P(t) = \int_{t0}^{t}\int_{V_0} |\Psi(\boldsymbol{r},t)|^2\,\mathrm{d}V\,\mathrm{d}t$. t_0 is the time at which the measurement is started and $t \geqslant t_0$ is the measurement time. V_0 is the volume investigated. $P(t)$ is a fraction of $(t - t_0)$ [111].
- The dwell time probability density is $\int_{t0}^{t} |\Psi(\boldsymbol{r},t)|^2\,\mathrm{d}t$.
- The time-independent wavefunction of the Schrödinger equation is as follows: $\psi(\boldsymbol{r}, E) = \frac{1}{2\pi}\int_{-\infty}^{\infty} \exp(\mathrm{i}Et)\Psi(\boldsymbol{r},t)\,\mathrm{d}t$ (the time-to-energy Fourier transformation).

References

[1] García N 1977 *J. Chem. Phys.* **67** 897
[2] Stoll E, Baumberger M and García N 1984 *J. Chem. Phys.* **81** 1496
[3] Füstöss L and Varga G 1990 *Vacuum* **40** 47
[4] Varga G and Füstöss L 1990 *Vacuum* **41** 315
[5] Varga G and Füstöss L 1991 *Surf. Sci.* **243** 23
[6] Varga G and Füstöss L 1990 *11th Yugoslav Vacuum Congr.: Zveza Drustev za Vakuumsko Tehniko Jugoslavije* (Jugoslavian Vacuum Society, Jugoslavia, Ljubljana) vol 24, pp 382–90
[7] Varga G 1998 *Vacuum* **50** 339
[8] Salanon B and Armand G 1981 *Surf. Sci.* **112** 78
[9] Cabrera N, Celli V, Gooman F O and Manson R 1970 *Surf. Sci.* **19** 67
[10] Balázs E and Varga G 1987 *Vacuum* **37** 153
[11] Farías D and Rieder K H 1998 *Rep. Prog. Phys.* **61** 1575
[12] Gumhalter B 2001 *Phys. Rep* **351** 1
[13] Lina S Y, Hana K L and Zhang J Z H 2000 *Chem. Phys. Lett.* **324** 122
[14] Schinke R 1984 *J. Chem. Phys.* **80** 5510
[15] Clarke N J, Sironi M, Raimondi M, Kumar S, Gianturco F A, Buonomo E and Cooper D L 1998 *Chem. Phys.* **233** 9
[16] Zhang Y C, Tan Z, Zhang H, Zhang Q and Zhang J Z H 2000 *Chem. Phys.* **252** 191
[17] Domenico D, Hernández M I and Campos-Martínez J 2001 *Chem. Phys. Lett.* **342** 177
[18] Zhang Y C, Zhan L X, Zhang Q G, Zhu W and Zhang J Z H 1999 *Chem. Phys. Lett.* **300** 27
[19] Ehlotzky F 2001 *Phys. Rep.* **345** 175
[20] Ferrero M and Robicheaux F 2001 *Chem. Phys.* **267** 93
[21] Shen Z, Boustani I, Erdmann M and Engel V 2001 *Chem. Phys. Lett.* **339** 362
[22] Barinovs G, Markovic N and Nyman G 1999 *Chem. Phys. Lett.* **315** 282
[23] Kulander K C, Cerjan C and Orel A E 1991 *J. Chem. Phys.* **94** 2571
[24] Zhang H, Han Ke-Li, He Guo-Zhong and Lou Nan-Quan 1998 *Chem. Phys. Lett.* **289** 494
[25] Balakrishnan N, Alekseyev A B and Buenker R J 2001 *Chem. Phys. Lett.* **341** 594
[26] Mahapatra S, Köppel H, Cederbaum L S, Stampfuß P and Wenzel W 2000 *Chem. Phys.* **259** 211
[27] Sweeney C J and De Vries P L 1989 *Comput. Phys.* **January/February** 49
[28] De Raedt H 1996 Computer simulation of quantum phenomena in nano-scale devices *Annual Reviews of Computational Physics* vol 4, ed D Stauffer (Singapore: World Scientific) pp 107–146
[29] De Raedt H 1996 Quantum dynamics in nano-scale devices *Computational Physics* ed K-H Hoffmann and Schreiber (Berlin: Springer) pp 209–24
[30] De Raedt H and Michielsen K 1996 *Computer animation of electron motion in Nano-meter scale devices, in Proceedings IVMC '96* ed D Glazanov pp 51–7
[31] Andersson E and Stenholm S 2001 *Opt. Commun.* **188** 141
[32] Márk G I, Biró L P and Gyulai J 1998 *Phys. Rev.* B **58** 12 645
[33] Márk G I, Biró L P, Gyulai J, Thiry P A, Lucas A A and Lambin P 2000 *Phys. Rev.* B **62** 2797
[34] Márk G I, Biró L P and Lambin P 2001 *Modeling and Interpretation of STM Images of Carbon Nanotubes (NATO ARW) (Kiev, Sept. 2001)*
[35] Márk G I, webpage http://newton.phy.bme.hu/education/schrd/index.html

[36] Forenberg B 1975 *SIAM J. Numer. Anal.* **12** 509
[37] Ország S A 1980 *J. Comput. Phys.* **37** 93
[38] Feit M D, Fleck J A and Steiger A 1982 *J. Comput. Phys.* **47** 412
[39] Kosloff D and Kosloff R 1983 *J. Comput. Phys.* **52** 35
[40] Vasilyev O V and Paulocci S 1997 *J. Comput. Phys.* **138** 16
[41] Sahrakorpi S, webpage http://alpha.cc.tut.fi/∼sahrakor/research/teksti/teksti.htm
[42] Tal-Azer H and Kosloff R 1984 *J. Chem. Phys.* **81** 3967
[43] Kosloff D and Tal-Azer H 1993 *J. Comput. Phys.* **104** 457
[44] Askar A and Cakmark S 1978 *J. Chem. Phys.* **68** 2794
[45] Suzuki M 1985 *J. Math. Phys.* **26** 601
[46] Suzuki M 1990 *Phys. Lett.* A **146** 319
[47] Suzuki M 1991 *J. Math. Phys.* **32** 400
[48] Bandrouk A D and Shein H 1991 *Chem. Phys. Lett.* **176** 428
[49] Rouhi A and Wright J 1995 *Comput. Phys.* **9** 554
[50] Lánczos C 1950 *J. Res. NBS* **45** 255
[51] Park T J and Light J C 1986 *J. Chem. Phys.* **85** 5870
[52] Tal-Azer H, Kosloff R and Cerjan C 1992 *J. Comput. Phys.* **100** 179
[53] Gerber R B, Kosloff R and Berman M 1986 *Comput. Phys. Rep.* **5** 59
[54] Kosloff R 1988 *J. Phys. Chem.* **92** 2087
[55] Billing G D 1990 *Comput. Phys. Rep.* **12** 383
[56] Leforester C *et al* 1991 *J. Comput. Phys.* **94** 59
[57] Thaller B 2000 *Visual Quantum Mechanics* (Berlin: Springer) (ISBN 0-387-98929-3)
[58] Korolkov M V and Weitzel K M 2000 *Chem. Phys.* **252** 209
[59] Korolkov M V and Paramonov G K 1998 *Phys. Rev.* A **57** 4998
[60] Bisseling R N, Kosloff R and Manz J 1985 *J. Chem. Phys.* **83** 993
[61] Dattoli G, Mancho A M, Quattromini M and Torre A 2001 *Radiat. Phys. Chem.* **61** 99
[62] Palao J P and Muga J G 1998 *Chem. Phys. Lett.* **292** 1
[63] Jiang H and Zhao X S 2000 *Chem. Phys. Lett.* **319** 555
[64] Nest M, Kleinekathöfer U, Schreiber M and Saalfrank P 1999 *Chem. Phys. Lett.* **313** 665
[65] Mikhailova T Yu and Pupyshev V I 1999 *Phys. Lett.* A **257** 1
[66] Gollub D M and Richards D G 1996 Scattering of quantum wavepackets, physics on parallel computers *Project Description* Department of Physics and Astronomy, The University of Edinburgh, webpage http://ciphysik.uni-wuerzburg.de/∼dkgollub
[67] Richardson J L 1991 *Comput. Phys. Commun.* **63** 84
[68] Corey G C and Lemoine D 1992 *J. Chem. Phys.* **97** 4115
[69] Lemoine D 1997 *Comput. Phys. Commun.* **99** 297
[70] Varga G 2001 *Surf. Sci.* **482–5** 1152
[71] Varga G, webpage http://goliat.eik.bme.hu/∼vargag
[72] Burgoon J K, Bonito J A, Bengtsson B, Cederberg C, Lundeberg M and Allspach L 2000 *Comput. Human Behav.* **16** 553
[73] Murray-Smith D J 2000 *Math. Comput. Simul.* **53** 239
[74] Guantes R, Borondo F, Jaffé C and Miret-Artés S 1995 *Surf. Sci. Lett.* **338** L863
[75] Sanz A S, Borondo F and Miret-Artés S 2000 *Phys. Rev.* B **61** 7743
[76] Heller E J 1975 *J. Chem. Phys.* **62** 1544
[77] Sanz A S, Borondo F and Miret-Artés S 2001 *Europhys. Lett.* **55** 303
[78] Varga G 1999 *Surf. Sci.* **441** 472
[79] Estermann I and Stern O 1930 *Z. Phys.* **61** 953
[80] Estermann I, Frish R and Stern O 1931 *Z. Phys.* **73** 348
[81] Frish R and Stern O 1933 *Z. Phys.* **84** 430
[82] Varga G 1999 *Appl. Surf. Sci.* **144–5** 64
[83] Apel R, Farías D, Tröger H, Kristen E and Rieder K H 1996 *Surf. Sci.* **364** 303
[84] Poelsema B and Comsa G 1989 *Scattering of Thermal Energy Atoms from Disordered Surfaces* (Berlin: Springer)
[85] Patting M, Farías D and Rieder K H 2000 *Phys. Rev.* B **62** 2108
[86] Farías D, Patting M, Rieder K-H and Manson J R 2001 *Surf. Sci. Lett.* **480** L395
[87] Apel R, Farías D, Tröger H and Rieder K H 1995 *Surf. Sci.* **331–3** 57
[88] Farías D, Tröger H and Rieder K H 1995 *Surf. Sci.* **331–3** 150
[89] Farías D, Tröger H, Patting M and Rieder K H 1996 *Surf. Sci.* **352–254** 155

[90] Farías D, Patting M and Rieder K H 1997 *Surf. Sci.* **385** 115
[91] Carré M-N, Lemoine D, Picaud S and Girardet C 1996 *Surf. Sci.* **347** 128
[92] Lemoine D 1994 *J. Chem. Phys.* **101** 4343
[93] Heather R and Metiu H 1987 *J. Chem. Phys.* **86** 5009
[94] Lemoine D 1998 *Phys. Rev. Lett.* **81** 461
[95] Hernández M, Campos-Martínez J and Miret-Artés S 1994 *Phys. Rev.* B **49** 8300
[96] Miret-Artés S 1996 *Surf. Sci. Lett.* **366** L735
[97] Miret-Artés S 1996 *Surf. Sci. Lett.* **366** L681
[98] Guantes R, Borondo F, Jaffé C and Miret-Artés, 1994 *Int. J. Quantum Chem.* **52** 515
[99] Borondo F, Jaffé C and Miret-Artés 1994 *Surf. Sci.* **317** 211
[100] Miret-Artés S, Margalef-Roig J, Guantes R, Borondo F and Jaffé C 1996 *Phys. Rev.* B **54** 10 397
[101] Guantes R, Borondo F and Miret-Artés S 1997 *Phys. Rev.* E **56** 378
[102] Guantes R, Borondo F, Margalef-Roig J, Miret-Artés S and Manson J R 1997 *Surf. Sci. Lett.* **375** L379
[103] Guantes R, Borondo F and Jaffé C 1996 *Phys. Rev.* B **53** 14 117
[104] Hernández M, Serna S, Roncero O, Miret-Artés S, Villarreal P and Degado-Barrio G 1991 *Surf. Sci.* **251/252** 373
[105] de Andres P L and Vergés J A 1998 *Phys. Rev. Lett.* **80** 980
[106] Porter C E and Thomas R G 1956 *Phys. Rev.* **104** 483
[107] Efetov K B and Progodin V N 1993 *Phys. Rev. Lett.* **70** 1315
[108] Dyson F J 1962 *J. Math. Phys.* **3** 140
[109] Mehta M L 1991 *Random Matrices* 2nd edn (San Diego, CA: Academic)
[110] de Andres P L and Vergés J A 1999 *Phys. Rev.* B **59** 3086
[111] Balázs E, Varga G and Füstöss L 2001 *Surf. Sci.* **482–5** 1145
[112] Gumhalter B, Burke K and Langreth D C 1994 *Surf. Rev. Lett.* **1** 133
[113] Bilic A, Gumhalter B, Mix W, Golichowski A, Tzanev S and Snowdon K J 1994 *Surf. Sci.* **307–9** 165
[114] Gerber R 1987 *Chem. Rev.* **87** 29
[115] Siber A and Gumhalter B 1997 *Surf. Sci.* **385** 270
[116] Siber A and Gumhalter B 1998 *Phys. Rev. Lett.* **81** 1742
[117] Goldberger M L and Watson K M 1964 *Collision Theory* (New York: Wiley)
[118] Brenig W and Haag R 1959 *Fortschr. Phys.* **7** 183
[119] Bilic A and Gumhalter B 1995 *Phys. Rev.* B **52** 12 307
[120] Gumhalter B 1984 *Prog. Surf. Sci.* **15** 1
[121] Gumhalter B and Langreth D C 1999 *Phys. Rev.* B **60** 2789
[122] Siber A, Gumhalter B and Toennies J P 1999 *Vacuum* **54** 315
[123] Gumhalter B 1996 *Surf. Sci.* **347** 237
[124] Manthe U and Köppel H 1991 *Chem. Phys. Lett.* **178** 36
[125] Gross A 1998 *Surf. Sci. Rep* **32** 291
[126] Kroes G-J 1999 *Prog. Surf. Sci.* **60** 1
[127] Born M and Oppenheimer J R 1927 *Ann. Phys., NY* **84** 457
[128] Dreizler R M and Gross E K U 1990 *Density Functional Theory* (Berlin: Springer)
[129] Payne M C, Teter M P, Allan D C, Arias T A and Joannopoulos J D 1992 *Rev. Mod. Phys.* **64** 1045
[130] Kroes G J and Mowrey R C 1994 *J. Chem. Phys.* **101** 805
[131] Mowrey R C and Kroes G J 1995 *J. Chem. Phys.* **103** 1216
[132] Whaley K B, Yu C, Hogg C S, Light J C and Sibener S J 1985 *J. Chem. Phys.* **83** 4235
[133] Cvetko D, Morgante A, Santaniello A and Tommasini F 1996 *J. Chem. Phys.* **104** 7778
[134] Bertino M F, Hofmann F and Toennies J P 1997 *J. Chem. Phys.* **106** 4327
[135] Bertino M F, Manson J R and Silvestri W 1998 *J. Chem. Phys.* **108** 10 239
[136] Bertino M F, Graham A P, Rusin L Y and Toennies J P 1998 *J. Chem. Phys.* **109** 8036
[137] Boato G, Cantini P and Mattera L 1974 *Japan. J. Appl. Phys.* **2** 553
[138] Bertino M F, Glebov A L, Toennies J P, Traeger F, Pijper E, Kroes G J and Mowrey R C 1998 *Phys. Rev. Lett.* **81** 5608
[139] Witte G and Bertino M F 1997 *Surf. Sci.* **385** 1984
[140] Bertino M F, Miret-Artés S, Toennies J P and Benedek G 1997 *Surf. Sci.* **377** 714
[141] Bertino M F, Miret-Artés S and Toennies J P 1998 *Chem. Phys. Lett.* **287** 663
[142] Dai J and Light J C 1997 *J. Chem. Phys.* **107** 1676
[143] Hammer B, Scheffler M, Jacobsen K and Norskov J K 1994 *Phys. Rev. Lett.* **73** 1400
[144] Diño W A, Kasai H and Okiji A 1996 *Surf. Sci.* **363** 52
[145] Harris D C, Darling G R and Holloway S 1999 *Surf. Sci.* **433–5** 838

[146] Billing G D 1993 *Numerical Grid Methods and their Application to Schrödinger's Equation* ed C Cerjan (Amsterdam: Kluwer)
[147] Kosloff R 1993 *Numerical Grid Methods and their Application to Schrödinger's Equation* ed C Cerjan (Amsterdam: Kluwer) p 175
[148] Darling G R and Holloway S 1994 *J. Chem. Phys.* **101** 3268
[149] McCormack D A and Kroes G-J 1998 *Chem. Phys. Lett.* 515
[150] Gross A and Scheffler M 1998 *Phys. Rev.* B **57** 2493
[151] Miura Y, Kasai H, Diño W A and Okiji A 1999 *Surf. Sci.* **438** 254
[152] Diño W A, Kasai H and Okiji A 2001 *Appl. Surf. Sci.* **169–70** 36
[153] Miura Y, Kasai H, Diño W A and Okiji A 2001 *Surf. Sci.* **493** 298
[154] Miura Y, Diño W A, Kasai H and Okiji A 2001 *Surf. Sci.* **482–5** 306
[155] Thareja S and Sathyamurthy N 1989 *J. Indian Chem. Soc.* **66** 596
[156] Bejan D, Raesev G and Monnerville M 2001 *Surf. Sci.* **470** 293
[157] Jackson B and Lemoine D 2001 *J. Chem. Phys.* **114** 474
[158] Lemoine D and Jackson B 2001 *Comput. Phys. Commun.* **137** 415
[159] Pijper E, Somers M F, Kroes G J, Olsen R A, Baerends E J, Busnengo H F, Salin A and Lemoine D 2001 *Chem. Phys. Lett.* **347** 277
[160] Diño W A, Fukutani K, Okano T, Kasai H, Okiji A, Farías D and Rieder K-H 2002 *J. Phys. Soc. Japan* **70** at press